Quantitative Three-Dimensional Imaging of Live Avian Embryonic Morphogenesis Via Micro-computed Tomography

Alyssa L. Henning,[1] Michael X. Jiang,[1] Huseyin C. Yalcin,[2] and Jonathan T. Butcher[1]*

Many clinically relevant congenital malformations arise during mid to late embryonic stages. This period is challenging to image quantitatively in live embryos, necessitating the use of multiple specimens with increased experimental variability. Here we establish X-ray and blood-pool computed tomography (CT) contrast agent toxicity and teratogenesis thresholds for 3D Micro-CT imaging of live avian embryos. Day 4 chick embryos micro-injected with Visipaque™ (VP) developed for an additional 6 days without defect. X-ray radiation up to 798 mGy was nontoxic. Peak average contrast of 1,060 HU occurred within 1 hr of imaging at 50 μm resolution. VP-enhanced contrast persisted past 24 hr with delayed accumulation in the allantois. Regional volumes of VP-injected embryos were statistically identical to those of fixed embryos perfused with osmium tetroxide. We further quantified longitudinal volumetric morphogenesis of the allantois over 30 hr. These results demonstrate the safety and efficacy of contrast enhanced quantitative micro-CT imaging for live embryos. *Developmental Dynamics 240:1949–1957, 2011.* © 2011 Wiley-Liss, Inc.

Key words: contrast agent; development; heart; brain; toxicity; radiation; teratogen; defect; dosage; biodistribution; iodine; allantois; clearance

Accepted 2 June 2011

INTRODUCTION

Embryonic morphogenesis is a rapid and complex three-dimensional (3D) process by which the initially planar germ disc becomes a functioning organism many orders larger in size, with multiple interconnected networks of organs and tissues. Birth defects and preterm fetal demise are a consequence of genetic, epigenetic, and/or environmental changes during morphogenesis. While mutations affecting genes in very early patterning events are almost uniformly embryonically lethal, gestationally survivable but clinically serious malformations such as congenital cardiovascular defects arise during mid to late embryonic development when tissue primordia and their progenitor populations begin to differentiate and mature (Gilbert, 2006; Lloyd-Jones et al., 2010). Understanding the causal mechanisms of these defects and their functional sequellae are currently major research efforts. Many human organs, such as the heart, acquire nearly their adult morphology by the time they can be imaged non-invasively via ultrasound (Hornberger et al., 1996). A majority of the fundamental knowledge of vertebrate embryonic morphogenesis has been gained through studying vertebrate animal models, including zebrafish, chicks, and mice. Quantitative imaging technologies are essential to accurately identify mechanisms of normal 3D tissue morphogenesis and to compare the effects of genetic mutations or experimental treatments. Direct observation of dynamic cellular patterning and live embryonic morphogenesis is possible for early embryonic events using

[1]Department of Biomedical Engineering, Cornell University, Ithaca, New York
[2]Department of Mechanical Engineering, Dogus University, Istanbul, Turkey
Grant sponsor: American Heart Association; Grant number: 0830384N; Grant sponsor: National Science Foundation (CAREER award); The Hartwell Foundation; The LeDucq Foundation; Hunter R. Rawlings III Cornell Presidential Research Scholars Program; Cornell University Engineering Learning Initiatives Program.
***Correspondence to: Jonathan T. Butcher, Department of Biomedical Engineering, 304 Weill Hall, Cornell University, Ithaca NY 14853-7501. E-mail: jtb47@cornell.edu**

DOI 10.1002/dvdy.22694
Published online 13 July 2011 in Wiley Online Library (wileyonlinelibrary.com).

optical imaging (Zamir et al., 2006), but technologies for later stages have been difficult to create because of the requirements of breadth of field (order of cm^3) and spatial resolution (less than 100 μm) (Jones et al., 2005; Yalcin et al., 2010b; Kim et al., 2011). Optical imaging of thin histological sections generates high spatial resolution in the sectioning plane, but reconstructing the third dimension through serial sections is time-consuming and expensive, with much lower resolution than in the transverse plane. This is particularly problematic for resolving tortuous 3D anatomy common in embryos of these stages. Furthermore, the inability to obtain longitudinal data from the same embryo necessitates multiple experiments with separate embryos, increasing experimental variability. In vivo imaging technology such as ultrasound and micro-magnetic resonance imaging (micro MRI) can generate fully registered three-dimensional image datasets, but with a limited size of the imaging field, reduced spatiotemporal resolution, and/or low differential tissue contrast (Metscher, 2009b). Ultrasound is excellent for intracardiac hemodynamics in 2D with peak temporal resolutions of approximately 200 Hz and spatial resolution of 30–50 μm (Butcher et al., 2007; McQuinn et al., 2007). Achieving high 3D spatial resolution with ultrasound is currently limited by the mechanics of the ultrasound probe design, whether it is swept source or phased array (Nieman and Turnbull, 2010; Moran et al., 2011). Magnetic-field-based tissue contrast enhancement without the need for exogenous contrast agents is attractive, but the high imaging costs exceeding $400/hr (Kim et al., 2011) are prohibitive for widespread use. The spatial resolution of micro-MRI systems is tied directly to the bore size, thus limiting the breadth of view. New phased array systems enable simultaneous, multipoint dynamic imaging at improved spatial resolution and signal-to-noise ratio (Aristizabal et al., 2006), but still exhibit limited depth of field in comparison to micro-computed tomography (6 vs. 80 mm). Other in vivo systems used for quantitative imaging of embryonic morphogenesis include optical coherence tomography (OCT) and multiphoton laser microscopy (Jenkins et al., 2007; Yalcin et al., 2011). Though offering much higher spatial resolution (<10 μm), the inherent depth penetration limitations of these approaches (2–3 mm) constrain applications to early embryonic morphogenesis or small subsets of tissues (Liebling et al., 2005; Gargesha et al., 2009; Yalcin et al., 2011).

Micro-computed tomography (micro-CT) has emerged as a promising quantitative imaging modality for embryonic morphogenesis, as it can scan specimens within minutes at higher spatial resolutions and with lower cost per scan (Kim et al., 2011). Recent advances in CT contrast media (including osmium tetroxide [OT], Lugol's solution, iodine potassium iodide, gallocyanin-chromalum, and phosphotungstic acid stains) opacify soft tissues under X-rays (Bentley et al., 2007; Metscher, 2009a; Kim et al., 2011). Osmium tetroxide and Lugol's solution diffuse into tissues, developing contrast in the matrix but not in lumen spaces. Results from previous studies identified osmium tetroxide as the best non-proprietary option, offering high CT contrast intensity and clear identification of tissue boundaries (Johnson et al., 2006; Metscher, 2009b). However, these agents are embryotoxic, limiting imaging to fixed specimens. Non-invasive live imaging can detect primary developmental defects as they occur at the tissue and organ levels (Hogers et al., 2009) and follow their consequences over time qualitatively and quantitatively (Kim et al., 2011). Winkelmann and Wise reported the use of Omnipaque™ (iohexol) (OP) as an in vivo CT contrast agent to visualize rabbit and rat placentas (Winkelmann and Wise, 2009), and Visipaque™ (iodixanol) (VP) has been used to quantify the kidney volumes in mice (Almajdub et al., 2008) and to image human coronary arteries in vivo (van Soest et al., 2010). Micro-CT imaging, however, has not been applied to live embryos to date.

In this study, we address three major questions in evaluating the safety and efficacy of live embryonic imaging via micro-CT: (1) How does micro-CT X-ray radiation dose affect embryonic viability and morphogenesis? (2) How does CT contrast agent type and microinjected dose affect embryonic viability and morphogenesis? (3) How does CT contrast bio-distribute and persist within an embryo? Chick embryos were chosen for this study because they (1) have a 4-chambered heart with valves, (2) can be cultured almost to hatching completely in ovo, (3) tolerate biochemical and invasive microsurgical experimentation, and (4) form efficient transplantation chimera with quail and mice. We demonstrate that hyperosmotic blood pool contrast agent OP was embryotoxic, but iso-osmotic contrast agent VP was not embrotoxic and did not cause any morphological defects. VP-enhanced micro-CT imaging resulted in time dependent contrast persistence that varied with tissue region. We also identified that CT contrast became sequestered in the allantoic vasculature and eventually cleared through this network. Finally, we determine that 3D volumetric quantification of contrast-enhanced tissues in live embryos was identical to that from fixed tissue specimens. These results, therefore, demonstrate that micro-CT can be used for quantitative imaging analyses of live avian embryo morphogenesis.

RESULTS

In Vivo Imaging With Visipaque and Micro-CT X-Ray Is Nontoxic

To assess the acute effects of the microinjection process on embryonic cardiovascular health, heart rates were taken immediately before injection (0−), immediately after injection (0+), 1 hr post-injection, and 24 hr post injection (Fig. 1A). Exposure to room environmental conditions and microinjection caused embryonic heart rates to drop significantly ($P < 0.01$) from 175 ± 8 bmp to 95 ± 15 bpm (EBSS 10 μL), from 183 ± 6 bpm to 79 ± 12 bmp (VP 10 μL), from 167 ±2 bpm to 113 ± 5 bpm (EBSS 15 μL), and from 188 ± 15 bpm to 105 ± 11 bpm (VP 15 μL). Heart rates, however, fully recovered within 1 hr (191 ± 5, 185 ± 8, 167 ± 5, and 173 ± 28 bpm for EBSS 10 μL, VP 10 μL, EBSS 15 μL, and VP 15 μL, respectively; Fig. 1A). This transient dip in heart rate was similar to that of other experimental interventions in the chick that did not result in developmental malformations (Groenendijk et al., 2008).

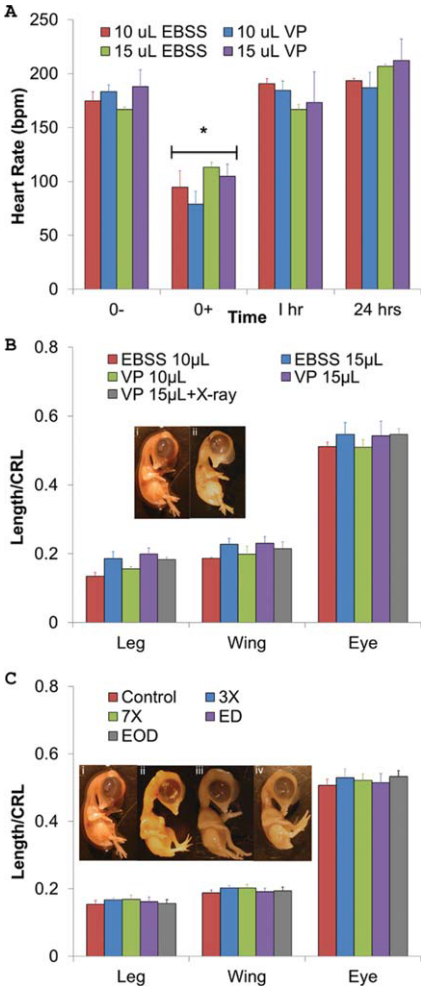

Fig. 1. **A:** Acute embryonic heart rate adaptation to CT contrast microinjection. An acute drop in heart rate occurs after injection (0+) of VP and EBSS ($P < 0.01$), but heart rates return to initial levels within 1 hr. n = 3, 7, 3, and 6 embryos, L to R. **B:** VP causes no morphological defects. Day 10 limb length, wing length, and eye perimeter for each embryo were normalized by their respective crown-rump lengths (CRL). Legend indicates volume of either EBSS or VP injected. VP 15 µL + X-ray includes 1× X-ray (114 mGy of radiation). No significant differences were found. Day 10 embryos are (i) control and (ii) VP 15 µL + X-ray. **C:** X-ray radiation causes no morphological defects up to 798 mGy doses. Identical measurements were taken as in Figure 1B. Treatments groups were as follows: imaged every day (ED), imaged every other day (EOD), imaged once on Day 4 at three times the dose (342 mGy, 3×), and imaged once at Day 4 at seven times the dose (798 mGy, 7×). There were no statistically significant differences in embryo morphology across limbs and X-ray treatments. Day 10 embryos are (i) control, (ii) ED, (iii) EOD, and (iv) 7×.

All embryos injected with hyperosmotic OP died within 24 hr, regardless of dose (Table 1). In contrast, 17 of 19 embryos injected with iso-osmotic VP survived until our experimental endpoint (Day 10), statistically identical to control embryo cultures (Table 1). We next quantified embryonic morphology in Day 10 embryos to test whether VP injection induced malformations. All wing and limb digits were present in their proper anatomical positions, and maxillofacial structures were properly formed. Also, the vitelline vasculature network expanded normally, and all pulmonic and aortic arch arteries formed in their proper positions. Therefore, no gross malformations occurred (Fig. 1B). Wing length, limb length, and eye perimeter, when normalized to crown-rump length, were statistically identical between VP and EBSS control injections at all doses tested (Fig. 1B), suggesting normal embryonic growth patterns were also maintained.

TABLE 1. Exogenous Contrast and X-Ray Dose Toxicity

Treatment	n	3D	6D	*P*
Control	8	7	7	—
1X EOD X-ray	8	8	8	0.317
1X ED X-ray	8	8	8	0.317
3X X-ray	8	7	7	1.000
7X X-ray	8	7	6	0.564
OP 5 µL	15	4	0	0.016
OP 10 µL	21	0	0	0.015
VP 5 µL	5	5	5	0.429
VP 10 µL	6	6	5	0.737
VP 15 µL	8	8	7	1.000
VP 15 µL+ X-ray	4	4	4	0.480

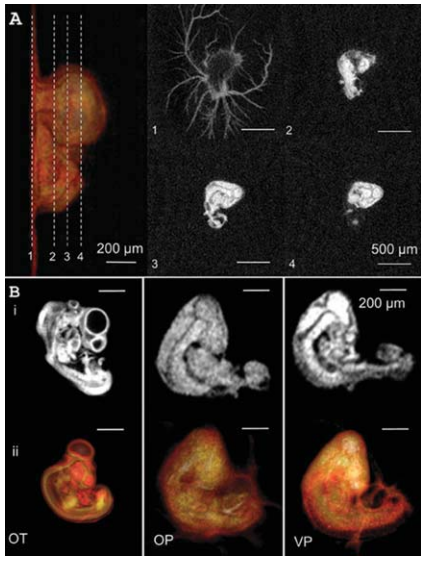

Fig. 2. **A:** 3D surface rendering (far left) and 2D cross-sections of embryo (1–4) injected with 15 µL of VP. **B:** (i) 2D and (ii) 3D-rendered images of organs and vasculature using (OT) fixed-slice OT, (OP) injected Omnipaque™-350 iohexanol (10 µL), and (VP) injected Visipaque™-270 iodixanol (10 µL).

We then tested whether X-ray radiation dose induced developmental defects in live chick embryos. No statistical differences were observed in the survival of embryos treated with X-ray in comparison to controls (Table 1). As with VP injection, no morphological defects were observed at any radiation dose, as all embryos contained requisite number and patterning of digits, outflow vessels, maxillofacial structures, musculoskeletal tissues, and vitelline vasculature network growth (Fig. 1C). The length of embryonic limbs, wings, and eye size were statistically identical between all X-ray doses and untreated controls. Based on these results, we assert that X-ray radiation at doses up to 798 mGy (the amount of radiation that an embryo would be exposed to if it was imaged every day from Day 4 to Day 10 at 50 µm voxel resolution) does not adversely affect survival or tissue morphology. Furthermore, this X-ray dose was safe even if applied in one acute bolus (7×). We further tested if combined X-ray and VP microinjection was toxic. Four embryos were injected with 15 µL of VP and underwent one micro-CT scan at 114 mGy. These embryos all survived until Day 10 (Fig. 1B) with normal morphology (Fig. 1C). Taken together, these results support that the in vivo micro-CT imaging process, from microinjection to CT imaging, has no effect on embryonic chick vitality and morphology.

Time Dependency of Organ-Specific CT Contrast

The extraembryonic vasculature, forebrain, hindbrain, body, and vascularized tissues were visible by micro-CT within 15 min of microinjection. Tissues with limited vascularity such as the limbs and wings of Day 4 chick embryos were only partially visible (Fig. 2A, B). These results were in contrast to our previous results in fixed embryos with osmium tetroxide (OT), which revealed the limbs but not the allantois (Fig. 2B) (Kim et al., 2011). Next, we quantified the intensity and biodistribution of CT contrast in live chick embryos up to 30 hr post-injection (Day 5.5). The lowest consistently detectable contrast threshold was approximately 150 HU, which was surpassed by both VP and OP regardless of injected dose (Fig. 3). Fifteen-microliter VP-injected doses generated significantly higher CT contrast in the heart and dorsal aorta than those imaged with only a 10-μL dose ($P < 0.05$, Fig. 3A), likely because those regions contain the most lumen space of those tested. Fixed embryos perfused with OT (the "gold standard") exhibited the highest heart and limb CT contrast overall ($P < 0.01$, Fig. 3A), and OT was the only agent to create significantly different tissue-specific CT intensity signatures ($P < 0.01$). However, as shown in Figures 2B and 3B, tissue boundaries were clearly delineated by VP at early time points, enabling volumetric quantification. Vitelline vasculature contrast was eliminated within the first 2 hr, while embryonic tissue CT contrast intensity decreased exponentially over time. VP at 10 μL did not persist in tissues past approximately 12 hr, whereas VP at 15 μL remained in embryos up to 36 hr after microinjection (Fig. 3B, C). Within 1 hr after injection, the contrast was highest in the brain (1,060 ± 170 HU), followed by the dorsal aorta (970 ± 160 HU), then by the heart (950 ± 190 HU), then by the limb bud (790 ± 120 HU), and finally by the allantois (150 ± 80 HU). The contrast in the brain, dorsal aorta, heart, and limb all decreased according to first order dynamics with r^2 values of 0.980, 0.994, 0.966, 0.991, and time constants of 6.17, 5.25, 4.67, and 5.25 hr, respectively. Surprisingly, the allantois increased in CT contrast, peaking at 9 hr post-injection (545 ± 220 HU) before decreasing again over time. Contrast persisted in the allantois (190 ± 130 HU) even after 30 hr when all the other regions were unrecognizable from background. We fit allantoic contrast kinetics to a model combining power growth and exponential decay with ($R^2 = 0.841$) and

$$c = 256t^{0.549} \times e^{\frac{-t}{14.6}}$$

where c is the contrast value and t is time in hours (Fig. 3B).

Tissue-specific peak CT contrast values were then compared at early (0–2 hr), middle (8–9 hr), and late time points (22–30 hr, Fig. 3C). The allantois has significantly less contrast relative to other areas of the body at early time points ($P < 0.01$), but at later time points, the allantois is more highly contrasted than other regions ($P < 0.05$), indicating that VP gradually disappears from internal organs and accumulates in the allantois over time. Additionally, allantois contrast at 8–9 hr is greater than contrast at early and late time points ($P < 0.01$ and $P < 0.05$, respectively), showing that this organ is most visible around 8 hr after injection. Heart contrast at early time points was significantly higher than that at middle and later time points ($P < 0.01$). Limb, dorsal aorta, and brain contrasts all reduce significantly with time ($P < 0.01$, early vs. middle and early vs. late; $P < 0.05$, middle vs. late) in an exponential manner, but no significant differences in intra-embryonic tissue contrast occurred with VP at any time point. These results suggest that tissue contrast enhancement occurs mostly through circulation and less through diffusion. Passive extravasation through the vitelline vasculature appears to be the main mode of embryonic clearance of contrast, but sequestration in the allantois is also important.

Micro-CT Derived Tissue Volumes From Live Embryos Are Comparable to Those of Fixed Tissue Specimens

Based on our results from multiple image sessions, tissue/organ boundaries for volumetric measurement remain detectable up to 3 hr post-injection. 3D volumes of sample CT visible tissues (the forebrain, midbrain, eye, and heart) injected with VP (n=5) and treated with OT (n=3) were quantified and compared (Fig. 4A). The brain, eye, and heart images were bright, high-attenuating regions in embryos injected with VP. In contrast, these regions were dark and thus non-attenuating in embryos stained with OT (Fig. 2B). The larger standard deviations in VP volume measurements reflect a somewhat greater ambiguity of boundaries between the brighter organs and surrounding tissue. For example, whereas the two-lobed structure of the forebrain could be distinguished in both cases, the space between the two lobes in the midbrain was only identifiable in embryos treated with OT (Fig. 4A). Regardless, the measured 3D volumes were statistically identical between all analyzed organs: the forebrain of embryos injected with VP (0.51 ± 0.21 mm^3) and those treated with OT (0.66 ± 0.09 mm^3), the midbrain for embryos injected with VP (3.04 ± 0.95 mm^3) and those treated with OT (3.23 ± 0.24 mm^3), and the eye for embryos injected with VP (0.89 ± 0.178 mm^3) and those treated with OT (0.92 ± 0.37 mm^3). The total heart volume (including lumen and myocardial tissue) was also very close between embryos injected with VP (1.75 ± 0.75 mm^3) and those treated with OT (1.85 ± 0.05 mm^3).

During longitudinal imaging of the same embryo using micro-CT, we noted that the allantois increased in size over time. We therefore quantified the volume of allantoic morphogenesis over a 30-hr period (Fig. 4B) and found a linear increase in average allantois volume from Day 4 to Day 5 with time ($V = 0.894t + 1.101$, $R^2 = 0.874$), where V is the volume (mm^3) of the allantois and t is the time in hours.

DISCUSSION

Quantitative multidimensional imaging is critically important for establishing normal and malformed tissue patterns associated with genetic and environmental factors. While many early morphogenetic events such as gastrulation and neurulation can be clearly observed in cultured embryos

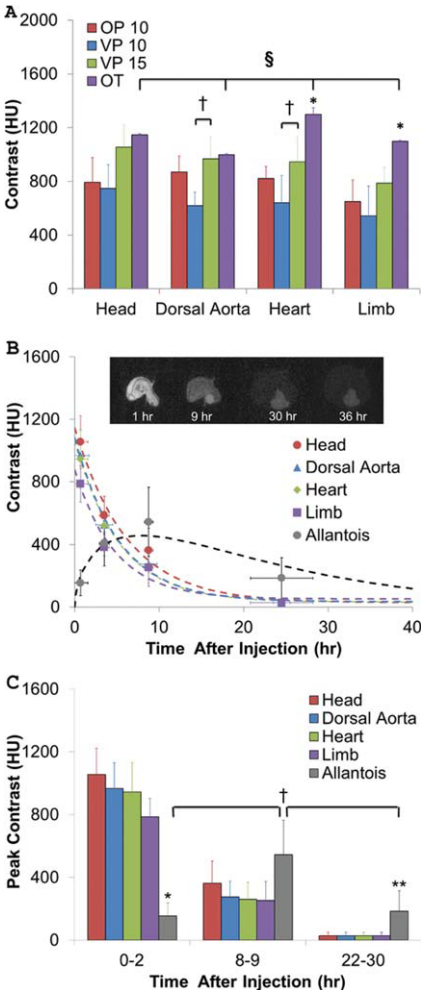

Fig. 3. Comparison of CT contrast enhancement. **A:** In vivo scans were taken within 1 hr after injection of contrast agents: 10 μL OP, 10 μL VP, and 15 μL VP. Peak contrast values were measured using MicroView and compared to those of OT. n = 4, 3, 5, and 3 from left to right. †$P < 0.05$ with respect to dose volume; *$P < 0.01$ with respect to all other contrast types; §$P < 0.01$ between anatomical regions with OT. **B:** Nonlinear regressions of VP contrast degradation in each anatomical region. Inset (i–iv): serial images from the same Day 4 chicken embryo at hours indicated. **C:** Comparison of peak regional contrasts over time. *$P < 0.01$ with respect to all other tissues at 0–2 hr; **$P < 0.05$ with respect to all other tissues at 22–30 hr; †$P < 0.05$ with respect to other time points.

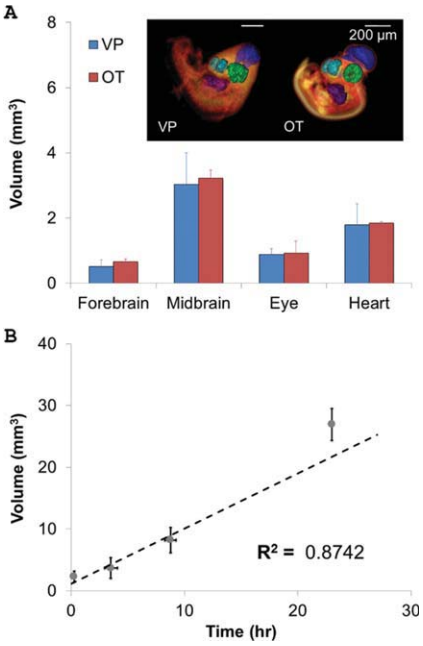

Fig. 4. **A:** Comparison of quantitative volumetric data of Day 4 embryos imaged in vivo (VP) and ex vivo (OT). The colors for each region are as follows: dark blue, hindbrain; light blue, forebrain; green, eye; purple, heart. No significant differences in organ volume were found. n = 3 and 5 for OT and VP, respectively. **B:** Average volumes of VP-contrasted fluid in the allantois at 0–2, 3–4, 8–9, and 22–30 hr after VP injection (n = 5). Allantois volume increases linearly at a rate of 0.894 mm^3/hr.

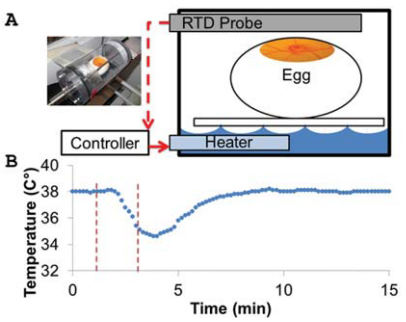

Fig. 5. Controlled environment chamber maintains temperature, enabling micro-CT imaging in vivo. **A:** Controlled environment system components. See text for details. **B:** Temperature-time profile during the process of adding an embryo into the housing.

with a variety of optical techniques (Liebling et al., 2005; Gargesha et al., 2009), the vast majority of gestationally survivable yet clinically serious defects arise during mid to late embryonic stages where these imaging techniques have limited effectiveness (Hogers et al., 2009; Kim et al., 2011). Non-invasive 3D imaging is a powerful approach for quantitative visualization, but its application to live embryos has been limited due to long scan times (thus cost and morphological drift), spatial resolution (both breadth of view and voxel size), toxicity of the imaging protocol, and limited soft tissue contrast. In this study, we establish and validate the first quantitative volumetric imaging study in live embryos using micro-CT. We show that iodixanol (Visipaque^{TM}) up to 10% of circulating blood volume (Rychter et al., 1955) and X-ray radiation of at least 798 mGy is non-embryotoxic and non-teratogenic for live chicken embryos. We determine that CT contrast persists for up to 30 hr, enabling longitudinal quantitative analysis of embryonic morphogenesis.

Ultrasound and/or micro-MRI are currently the standard imaging modalities for quantitative imaging of live embryos. Micro-MRI has seen significant use for quantitative volumetric analysis of avian, murine, and xenopus embryos (Ahrens et al., 2006; Pallares et al., 2009; Nieman and Turnbull, 2010). In reference to the current study, micro-MRI has been used to image quail embryo heart development in 3D (Bain et al., 2007; Hogers et al., 2009; Duce et al., 2011). Duce et al. (2011) report that the sagittal crown rump length in Japanese quail was 7 and 10 mm at Day 4 and Day 5, respectively. Total embryo volume was 0.038 mL at Day 4, and it increased to 0.105 mL at Day 5. Quails were visible in ovo from Day 3 and later, and 3D image rendering enabled vessels, the spine, the brain, and eyes to be seen clearly (Duce et al., 2011). Bain et al. (2007) measured brain, heart, and liver volumes in quail from Day 12 to Day 20 using MRI and reported an increase in brain volume from 0.4 to 1.0 cm^3, an increase in liver volume from 0.2 to 0.8 cm^3, and an increase in heart volume from 0.1 to 0.5 cm^3. They also noted that heart volumes for wild type quail embryos were smaller than those imaged via MRI because the blood within the heart chambers was included in the MRI volume measurement (Bain et al., 2007). Even with high field strengths, micro-MRI requires tenfold longer scanning time in contrast to micro-CT (21 vs. 2 min) for avian embryos (Hogers et al., 2009). These quail embryos were also scanned at low temperatures (4°C for 1 hr; Hogers et al., 2009) to limit motion artifacts, albeit at the risk of malformations (De la Cruz et al., 1966). With respect to possible defects caused by the imaging process, Hogers et al. (2009) tracked quail embryo development in vivo via MRI and performed similar morphological

TABLE 2. In Vivo Micro-CT Contrast Agents Used to Image Adult Mice

Agent	Subject	Contrast in aorta	Concentration (mgI/mL)	Dose	Osmolarity	Persistence	LD50	Reference
Isovue	Mouse	500 HU	370	1 mL/ hr, constant infusion	Low	10 min	21.8 gI/kg	Badea et al., 2004
Fenestra-VC	Mouse	620 HU	50	500 μL/ 25 g	Iso-osmolar	3 hr	>5,000 mg/kg	Badea et al., 2004
eXIA 160	Mouse	900 HU	20	200 μL/ 20 g	—	1 hr, 500HU	25 mL/kg	Prajapati and Keller, 2011
Omnipaque	Mouse	—	300	250 μL	Low	30 min	24.2 gI/kg	Paulus et al., 2000
Omnipaque	Chicken embryo	870 HU	350	10 μL	Low	—	—	Current study
Visipaque	Mouse	—	320	8 μL/ g	Iso-osmolar	35 min	15–20 gI/kg	Almajdub et al., 2008
Visipaque	Chicken embryo	970 HU	270	15 μL	Iso-osmolar	3 hr	—	Current study

studies to ours. They measured embryonic length (vertical distance from the top of the head to the tail) in vivo, compared their results to published growth curves, and also compared wet weights of control embryos to imaged embryos. Like us, they found no evidence of slowed development and morphological defects after imaging (Hogers et al., 2009). Heidrich and colleagues conducted the only previous prenatal in vivo imaging study with micro-CT using chicken embryos but focused on bone development in fetal stages (Day 10–18) where endogenous CT attenuation occurred (Heidrich et al., 2011). No visualization of soft tissues was achieved in this study. The authors showed short-term viability with imaging under anesthetization, but longer-term viability is unknown.

Because embryonic soft tissues do not attenuate X-rays, exogenous contrast is required. A number of agents have been used, including Microfil (Butcher et al., 2007; Yalcin et al., 2011), potassium iodide, Lugol's solution, phosphotungstic acid (Metscher, 2009b), and osmium tetroxide (Kim et al., 2011), but for nonliving fixed specimens. In vivo micro-CT blood pool contrast agents, including Fenestra VC™, Isovue™, Omnipaque™, and Visipaque™, have not been previously evaluated in embryos, but they have been used in adult mice (Table 2). Almajdub and coworkers used Visipaque™-320 to visualize mouse kidneys and reported that the VP was cleared from mice via the renal system in 35 min (Almajdub et al., 2008). As in our chicken embryos, the renal vasculature was significantly enhanced at early imaging time points, while poorly vascularized areas such as the pyramids of the renal medulla remained virtually invisible (Almajdub et al., 2008). Additionally, Hainfeld et al reported that OP was detectable in mouse kidneys 10 min after injection but was not quantifiable after 1 hr. Like the kidneys depicted by Almajdub et al. (2008), the renal artery and vein were highly visible. However, there was less distinction between the cortex and medulla (Hainfeld et al., 2006). In contrast to adults, embryonic blood rheology changes over morphogenesis (Yalcin et al., 2011). In these conditions, iso-osmotic VP did not induce toxicity while hyperosmotic OP did, which suggests that for future embryonic contrast strategies, osmolarity needs to be balanced.

CT contrast clearance in humans and adult mammals is achieved primarily through the renal system (Hainfeld et al., 2006; Almajdub et al., 2008; Badea et al., 2008). Clearance from embryos is poorly understood. In our study, we found that vitelline vasculature contrast dimmed first, followed by embryonic tissue contrast, and finally contrast in the allantois. The free iodixanol (VP) molecules used in our study were approximately 1–2 nm in size. The slower extravasation of VP through the allantoic vessel wall in comparison to vitelline vessels may reflect its decreased permeability (Zhang et al., 2008). Surprisingly, we quantified an increase in allantois contrast prior to decrease over time while all other regional contrasts were rapidly diminishing. Embryos first form a primitive clearance system with the rudimentary pronephros and mesonephros (Day 2) as well as the metanephros (also Day 2) and the allantois (Day 4), respectively (Romanoff, 1952; Bellairs and Osmond, 2005). This primitive system then undergoes extensive development between days 7 and 15, beyond the period of our live imaging, in which the pronephros and mesonephros degenerate, leaving the metanephros to form into a kidney (Narbaitz and Kapal, 1986; Clark et al., 1993; Navarro et al., 2003). One of the main functions of the allantois in early embryos (Day 4–5, like in our study) is to store and excrete nitrogenous metabolites that the embryo produces (Romanoff, 1967; Bellairs and Osmond, 2005). Additionally, allantoic sac fluid is hypo-osmotic in comparison to blood serum (Murphy et al., 1983; Graves et al., 1986). At Day 4, the fluid in the allantois is derived from the allantoic wall (Romanoff, 1952). Graves et al. also found that the allantoic epithelium becomes increasingly able to actively transport sodium from allantoic fluid (Graves et al., 1986). Active transport into this primitive renal system, potentially through an osmotic gradient, may also be occurring in the renal system to expel contrast agents from the body. At Day

5, mesonephric excreta begin to accumulate within the allantoic sac, and the sac also grows larger over time and begins to excrete wastes. Therefore, the mesonephric fluids and sac growth may dilute the concentration of contrast agent in the allanotic sac over time as the embryos grow from Day 4 to Day 5 (Romanoff, 1952). How these diverse mechanisms of molecular accumulation and removal within the primitive avian allantoic network interact is not yet known, and complete elucidation is beyond the scope of the current study.

We were able to quantify in real time the morphogenesis of the embryonic chick allantois. As observed by others, the allantois did not grow spherically (Bellairs and Osmond, 2005) (Fig. 3B), but rather extended cranially from the hindgut into the cavity of the chorion (Starck and Ricklefs, 1998). The linear increase in allantois volume we identify also agrees with previous qualitative observations on natural allantoic growth (Romanoff, 1967; Starck and Ricklefs, 1998). While the imaging methodology outlined here enables a nearly tenfold increase in micro-CT imaging time in embryonic compared to postnatal organisms, our results indicate that additional injections will likely be needed for multi-day quantitative longitudinal analyses. It remains to be seen whether contrast persistence will be maintained as renal and lymphatic functions are established. As advances in nanotechnology and molecular targeting improve, longer-term quantitative 3D studies from fewer injections will likely be enabled (Romanoff, 1967; Starck and Ricklefs, 1998; Mukundan et al., 2006). Micro-CT imaging will, therefore, become a powerful and more versatile tool enhancing experimental and genetic approaches to embryonic morphogenesis. These include dynamic analyses of cell-field-specific migrations, local delivery of genes or growth factors, and longitudinal fate mapping in 3D space. Nanoparticle contrast agents can also be developed to target specific sites in the body, but information is needed on where the particles localize. Animal models are essential in this regard, and micro-CT imaging will give us a very high-resolution framework to observe where the nanoparticles travel and how they function in the body. Our embryonic chick model may, therefore, be a versatile platform to evaluate the safety and efficacy of nanoscale CT contrast technologies.

In conclusion, we establish that micro-CT imaging is a promising research platform for quantitative morphogenesis in live embryos. To obtain the best brain, dorsal aorta, heart, and limb images in Day 4 embryos, scan as soon as possible after injecting, between 0 and 4 hr. For best results in the allantois, image embryos at 8 hours. To take full advantage of micro-CT for dynamic whole embryo imaging, two additional technologies are required: (1) gating technologies for embryos that lack an externally recordable ECG signal, and (2) injectable contrast media that better control diffusion and biodistribution. With respect to the first, techniques such as retrospective and prospective gating will allow us to better view the embryonic heart (Badea et al., 2008). Jenkins and colleagues obtained 3D and 4D images of avian hearts using optical computed tomography (Jenkins et al., 2007). For smaller organisms that do not provide a gating signal but produce periodic motion, Liebling et al. created a procedure to reconstruct 3D volumes based on information contained in sequences of 2D confocal microscope images (Liebling et al., 2005). Also, Holmes and coworkers were the first to report a self-gated cine MRI protocol in which a navigator signal was used after imaging to determine heartbeat and breathing cycles in chicken embryos in ovo, generating cardiac images that did not contain motion artifacts (Holmes et al., 2008). Additionally, Badea et al. performed cardiopulmonary imaging in mice by using X-ray tubes with exposure times that were short enough to minimize blurring in hearts and lungs during cardiac and breathing cycles (Badea et al., 2004). Regarding alternative CT contrast agents, Rabin and colleagues reported the use of polymer-coated bismuth sulfide nanoparticles to image blood vessels, the liver, and lymph nodes in mice. However, the effects that the nanoparticles may produce on organ development on the scale of days are uncertain (Rabin et al., 2006). As these strategies are realized, the adaptation of high-resolution quantitative live imaging technology and tailorable molecular imaging strategies will markedly expand the opportunities for fundamental and applied studies in embryonic development.

EXPERIMENTAL PROCEDURES

Environmental Culture System for Micro-CT Imaging of Avian Embryos

To maintain temperature and humidity around the embryo during the micro-CT imaging processes, we constructed a closed polycarbonate tube that fit inside the micro-CT machine. A contoured platform in the chamber held the embryo in place. We filled the tube with water up to the level of the platform and installed an immersible water heater controlled by an automated PID temperature controller, which heated up the water and, in turn, the air by passive convection. The air temperature was measured using an RTD probe, which was wired to the temperature controller (Fig. 5A). Once the temperature inside the chamber remained at 38°C for 2 min, the chamber was opened to admit the embryo. The air temperature then returned to 38°C with a time constant of 1 min and 50 sec (Fig. 5B).

In Vivo Contrast Agent Microinjection

Three-day incubated chicken embryos were cultured in ovo using a procedure adapted from Nakamura and Funahashi (2001). First, a small hole was made at the pointed end of the egg after wiping the shell down with a Kimwipe. Then 6 mL of albumin was pulled out with a 21-gauge needle. The hole was sealed with masking tape. Two large strips of masking tape were used to cover the top of the egg, and a window was created using curved dissecting scissors. Sterilized plastic wrap was then secured over the window with masking tape, allowing beating hearts to be seen without disturbing the wrap. The embryos were then placed in a 38°C incubator (no CO_2 control), and cultured for up to 7 additional days (stopping at Day 10). Borosilicate glass capillary tubes (Sutter Instruments,

OD 1.00 mm, ID 0.75 mm) were drawn into microneedles (Sutter Instruments p-97) with inner diameters of 20 μm and then beveled to approximately 45° with a microforge.

Microinjection was accomplished via a gravity-driven pressure gradient and a micromanipulator as described by Butcher et al. (2007). The pressure gradient was established by positioning a 3-mL syringe (BD) with a clamp at the top of a laboratory stand. Soft tissues were visualized by microinjection of circulating blood pool contrast agents, Omnipaque-350 iohexol (OP) or Visipaque-270 iodixanol (VP), through extraembryonic vessels. In preliminary experiments, FITC-Dextran was co-delivered to confirm via fluorescent microscope that a clean microinjection of CT contrast was achieved (Yalcin et al., 2010a). Embryos injected with equivalent volumes of EBSS (Sigma, St. Louis, MO) served as controls. For toxicity studies, embryo heart rates were taken per 15 sec inside the closed incubator before injection, 1 hr after injection, and 24 hr after injection.

X-ray and Contrast Agent Toxicity and Morphology

The toxicity of micro-CT X-ray radiation doses on chicken embryos from Day 4 to Day 10 was assessed with the aid of the controlled environment chamber. Each X-ray scan lasted 2 min and exposed embryos to three different doses of X-ray radiation, 1× (114 mGy), 3× (342 mGy), and 7× (798 mGy), where 1× constituted a standard 50-μm resolution scan for living specimens as measured by GE Healthcare technicians. Five different X-ray treatments were then applied: (1) scanned once every day until Day 10 (a total dose of 7×), (2) scanned once every other day to Day 10 (a total dose of 3×), (3) scanned once at 3× at Day 4, (4) scanned once at 7× at Day 4, and (5) a sham control group placed in the environmental control chamber without X-ray for 2 min.

Each embryo surviving to 10-day culture was removed from the egg, fixed in 4% paraformaldehyde, and analyzed morphologically using a V20 Stereomicroscope (Zeiss, Thornwood, NY). Crown-rump (CRL), limb, and wing lengths, as well as eye perimeter, were measured directly from images with ImageJ software (NIH). We defined "crown-rump" as the length of the line following the curvature of the back from the top of the head to the tip of the tail. The (left) wing length was measured from the middle of the elbow to the tip, following the contour of the wing. On the left, leg length was measured from the heel to the tip of the longest middle toe, following the contour of the leg. The eye perimeter was measured when the side of the head was level with the microscope stage. All measurements were normalized to CRL to account for normal variation in embryo size.

In Vivo Micro-CT Scanning

Each injected chicken embryo was taken from the incubator and placed in the controlled environment chamber once it was at a steady-state temperature of 38°C. Imaging was accomplished with a GE micro-CT scanner (GE Healthcare eXplore CT 120, Piscataway, NJ) at 50 μm resolution for 2 min with an X-ray radiation dose of 114 mGy. Post-processing, visualization, and image quantification were then performed using MicroView (GE Healthcare) and OsiriX. X-Ray attenuation through tissue (normally associated with its density) is registered by a gamma camera as contrast intensity. Chicken embryo contrast intensity grayscale values were converted to Hounsfield units (HU), which correlate with bone material density (Badea et al., 2008) via calibration with a micro-CT bone phantom (SB3, General Electric). The extraembryonic fluid space was used as a zero reference for analyses.

Contrast Measurement and Volume Quantification

Virtual cross-sections containing the brain, heart, dorsal aorta, and limb were analyzed via MicroView image reconstruction software to find the absolute difference in contrast from the baseline in Hounsfield Units (HU). MicroView files were then imported into OsiriX, where 3D isosurface renderings and virtual 2D slices were generated. To quantify organ volumes, region-growing algorithms (RGA, OsiriX) were applied as described in Kim et al. (2011).

Statistics

The non-parametric Kruskal-Wallace test was used to analyze heart rates across time and contrast agent. For contrast agent and X-ray radiation toxicity analysis, Pearson's Chi-squared test was performed. For all other data, one-way ANOVA was applied across all factors. The Tukey-Kramer post-hoc testing method was then applied, with $P < 0.05$ as significance thresholds. All data were reported as means + standard deviations.

ACKNOWLEDGMENTS

The authors thank Mark Riccio for his technical assistance in micro-CT scanning and image processing. J.T.B. was funded by the American Heart Association, National Science Foundation, The Hartwell Foundation, and the LeDucq Foundation. A.L.H. was funded by the Hunter R. Rawlings III Cornell Presidential Research Scholars Program. M.X.J. was funded by the Cornell University Engineering Learning Initiatives Program.

REFERENCES

Ahrens ET, Srinivas M, Capuano S, Simhan HN, Schatten GP. 2006. Magnetic resonance imaging of embryonic and fetal development in model systems. Methods Mol Med 124:87–101.

Almajdub M, Magnier L, Juillard L, Janier M. 2008. Kidney volume quantification using contrast-enhanced in vivo X-ray micro-CT in mice. Contrast Media Mol Imag 3:120–126.

Aristizabal O, Ketterling JA, Turnbull DH. 2006. 40-MHz annular array imaging of mouse embryos. Ultrasound Med Biol 32:1631–1637.

Badea C, Hedlund LW, Johnson GA. 2004. Micro-CT with respiratory and cardiac gating. Med Phys 31:3324–3329.

Badea CT, Drangova M, Holdsworth DW, Johnson GA. 2008. In vivo small-animal imaging using micro-CT and digital subtraction angiography. Phys Med Biol 53: R319–350.

Bain MM, Fagan AJ, Mullin JM, McNaught I, McLean J, Condon B. 2007. Noninvasive monitoring of chick development in ovo using a 7T MRI system from day 12 of incubation through to hatching. Journal of magnetic resonance imaging. JMRI 26:198–201.

Bellairs R, Osmond M. 2005. Atlas of chick development. New York: Elsevier Academic Press. 476p.

Bentley MD, Jorgensen SM, Lerman LO, Ritman EL, Romero JC. 2007. Visualization of three-dimensional nephron structure with microcomputed tomography. Anat Rec (Hoboken) 290:277–283.

Butcher JT, Sedmera D, Guldberg RE, Markwald RR. 2007. Quantitative volumetric analysis of cardiac morphogenesis assessed through micro-computed tomography. Dev Dyn 236:802–809.
Clark NB, Feng JQ, Murphy MJ. 1993. Renal clearance measurements of electrolytes in embryonic chickens. J Exp Zool 265:107–111.
De la Cruz MV, Campillo-Sainz C, Munoz-Armas S. 1966. Congenital heart defects in chick embryos subjected to temperature variations. Circul Res 18: 257–262.
Duce S, Morrison F, Welten M, Baggott G, Tickle C. 2011. Micro-magnetic resonance imaging study of live quail embryos during embryonic development. Magn Reson Imag 29:132–139.
Gargesha M, Jenkins MW, Wilson DL, Rollins AM. 2009. High temporal resolution OCT using image-based retrospective gating. Opt Express 17:10786–10799.
Gilbert S, editor.2006. Developmental biology. Sunderland, MA: Sinauer Associates, Inc. 785 p.
Graves JS, Dunn BE, Brown SC. 1986. Embryonic chick allantois: functional isolation and development of sodium transport. Am J Physiol 251:C787–794.
Groenendijk BC, Stekelenburg-de Vos S, Vennemann P, Wladimiroff JW, Nieuwstadt FT, Lindken R, Westerweel J, Hierck BP, Ursem NT, Poelmann RE. 2008. The endothelin-1 pathway and the development of cardiovascular defects in the haemodynamically challenged chicken embryo. J Vasc Res 45:54–68.
Hainfeld JF, Slatkin DN, Focella TM, Smilowitz HM. 2006. Gold nanoparticles: a new X-ray contrast agent. Br J Radiol 79:248–253.
Heidrich A, Wurbach L, Opfermann T, Saluz HP. 2011. Motion-artifact-free in vivo imaging utilizing narcotized avian embryos in ovo. Mol Imag Biol 13:208–214.
Hogers B, van der Weerd L, Olofsen H, van der Graaf LM, DeRuiter MC, Groot ACGD, Poelmann RE. 2009. Non-invasive tracking of avian development in vivo by MRI. NMR Biomed 22:365–373.
Holmes WM, McCabe C, Mullin JM, Condon B, Bain MM. 2008. Images in cardiovascular medicine. Noninvasive self-gated magnetic resonance cardiac imaging of developing chick embryos in ovo. Circulation 117:e346–347.
Hornberger LK, Need L, Benacerraf BR. 1996. Development of significant left and right ventricular hypoplasia in the second and third trimester fetus. J Ultrasound Med 15:655–659.
Jenkins MW, Chughtai OQ, Basavanhally AN, Watanabe M, Rollins AM. 2007. In vivo gated 4D imaging of the embryonic heart using optical coherence tomography. J Biomed Opt 12:030505.
Johnson JT, Hansen MS, Wu I, Healy LJ, Johnson CR, Jones GM, Capecchi MR, Keller C. 2006. Virtual histology of transgenic mouse embryos for high-throughput phenotyping. Plos Genet 2:471–477.
Jones EA, Baron MH, Fraser SE, Dickinson ME. 2005. Dynamic in vivo imaging of mammalian hematovascular development using whole embryo culture. Methods Mol Med 105:381–394.
Kim JS, Min J, Recknagel AK, Riccio M, Butcher JT. 2011. Quantitative three-dimensional analysis of embryonic chick morphogenesis via microcomputed tomography. Anat Rec (Hoboken) 294:1–10.
Liebling M, Forouhar AS, Gharib M, Fraser SE, Dickinson ME. 2005. Four-dimensional cardiac imaging in living embryos via postacquisition synchronization of nongated slice sequences. J Biomed Opt 10:054001.
Lloyd-Jones D, Adams RJ, Brown TM, Carnethon M, Dai S, De Simone G, Ferguson TB, Ford E, Furie K, Gillespie C, Go A, Greenlund K, Haase N, Hailpern S, Ho PM, Howard V, Kissela B, Kittner S, Lackland D, Lisabeth L, Marelli A, McDermott MM, Meigs J, Mozaffarian D, Mussolino M, Nichol G, Roger VL, Rosamond W, Sacco R, Sorlie P, Thom T, Wasserthiel-Smoller S, Wong ND, Wylie-Rosett J. 2010. Heart disease and stroke statistics: 2010 update: a report from the American Heart Association. Circulation 121:e46–e215.
McQuinn TC, Bratoeva M, Dealmeida A, Remond M, Thompson RP, Sedmera D. 2007. High-frequency ultrasonographic imaging of avian cardiovascular development. Dev Dyn 236:3503–3513.
Metscher BD. 2009a. MicroCT for comparative morphology: simple staining methods allow high-contrast 3D imaging of diverse non-mineralized animal tissues. BMC Physiol 9:11.
Metscher BD. 2009b. MicroCT for developmental biology: a versatile tool for high-contrast 3D imaging at histological resolutions. Dev Dyn 238:632–640.
Moran CM, Pye SD, Ellis W, Janeczko A, Morris KD, McNeilly AS, Fraser HM. 2011. A comparison of the imaging performance of high resolution ultrasound scanners for preclinical imaging. Ultrasound Med Biol 37:493–501.
Mukundan S, Jr., Ghaghada KB, Badea CT, Kao CY, Hedlund LW, Provenzale JM, Johnson GA, Chen E, Bellamkonda RV, Annapragada A. 2006. A liposomal nanoscale contrast agent for preclinical CT in mice. AJR Am J Roentgenol 186: 300–307.
Murphy MJ, Brown PS, Brown SC. 1983. Hydromineral balance during avian embryonic-development: effects of prolactin and growth-hormone. Am Zool 23: 898–898.
Nakamura H, Funahashi J. 2001. Introduction of DNA into chick embryos by in ovo electroporation. Methods 24:43–48.
Narbaitz R, Kapal VK. 1986. Scanning electron microscopical observations on the differentiating mesonephros of the chick embryo. Acta Anat (Basel) 125:183–190.
Navarro M, DeRuiter MC, Carretero A, Ruberte J. 2003. Microvascular assembly and cell invasion in chick mesonephros grafted onto chorioallantoic membrane. J Anat 202:213–225.
Nieman BJ, Turnbull DH. 2010. Ultrasound and magnetic resonance microimaging of mouse development. Methods Enzymol 476:379–400.
Pallares P, Fernandez-Valle ME, Gonzalez-Bulnes A. 2009. In vivo virtual histology of mouse embryogenesis by ultrasound biomicroscopy and magnetic resonance imaging. Reprod Fertil Dev 21:283–292.
Paulus MJ, Gleason SS, Kennel SJ, Hunsicker PR, Johnson DK. 2000. High resolution X-ray computed tomography: an emerging tool for small animal cancer research. Neoplasia 2:62–70.
Prajapati SI, Keller C. 2011. Contrast enhanced vessel imaging using microCT. J Vis Exp [DOI: 10.3791/2377].
Rabin O, Manuel Perez J, Grimm J, Wojtkiewicz G, Weissleder R. 2006. An X-ray computed tomography imaging agent based on long-circulating bismuth sulphide nanoparticles. Nat Mater 5:118–122.
Romanoff A. 1952. Membrane growth and function. Ann NY Acad Sci 55:288–301.
Romanoff A. 1967. Biochemistry of the avian embryo: a quantitative analysis of prenatal development. New York: John Wiley and Sons.
Rychter Z, Kopecky M, Lemez L. 1955. Micromethod for determination of the circulating blood volume in chick embryos. Nature 175:1126–1127.
Starck J, Ricklefs R. 1998. Avian growth and development: evolution within the altricial-precocial spectrum. New York:Oxford University Press. 456p.
van Soest G, Goderie T, Regar E, Koljenovic S, van Leenders GL, Gonzalo N, van Noorden S, Okamura T, Bouma BE, Tearney GJ, Oosterhuis JW, Serruys PW, van der Steen AF. 2010. Atherosclerotic tissue characterization in vivo by optical coherence tomography attenuation imaging. J Biomed Optics 15:011105.
Winkelmann CT, Wise LD. 2009. High-throughput micro-computed tomography imaging as a method to evaluate rat and rabbit fetal skeletal abnormalities for developmental toxicity studies. J Pharmacol Toxicol Methods 59:156–165.
Yalcin HC, Shekhar A, Nishimura N, Rane AA, Schaffer CB, Butcher JT. 2010a. Two-photon microscopy-guided femtosecond-laser photoablation of avian cardiogenesis: noninvasive creation of localized heart defects. Am J Physiol Heart Circ Physiol 299:H1728–1735.
Yalcin HC, Shekhar A, Rane AA, Butcher JT. 2010b. An ex-ovo chicken embryo culture system suitable for imaging and microsurgery applications. J Vis Exp [DOI: 10.3791/2154].
Yalcin HC, Shekhar A, McQuinn TC, Butcher JT. 2011. Hemodynamic patterning of the avian atrioventricular valve. Dev Dyn 240:23–35.
Zamir EA, Czirok A, Cui C, Little CD, Rongish BJ. 2006. Mesodermal cell displacements during avian gastrulation are due to both individual cell-autonomous and convective tissue movements. Proc Natl Acad Sci USA 103:19806–19811.
Zhang W, Chen Y, Swift MR, Tassi E, Stylianou DC, Gibby KA, Riegel AT, Wellstein A. 2008. Effect of FGF-binding protein 3 on vascular permeability. J Biol Chem 283:28329–28337.